Supporting Information

Ni nanoparticles/$V_4C_3T_x$ MXene heterostructures for electrocatalytic nitrogen fixation

Cheng-Feng Du, Lan Yang, Kewei Tang, Wei Fang, Xiangyuan Zhao, Qinghua Liang, Xianhu Liu, Hong Yu, Weihong Qi,* and Qingyu Yan**

Table of Contents

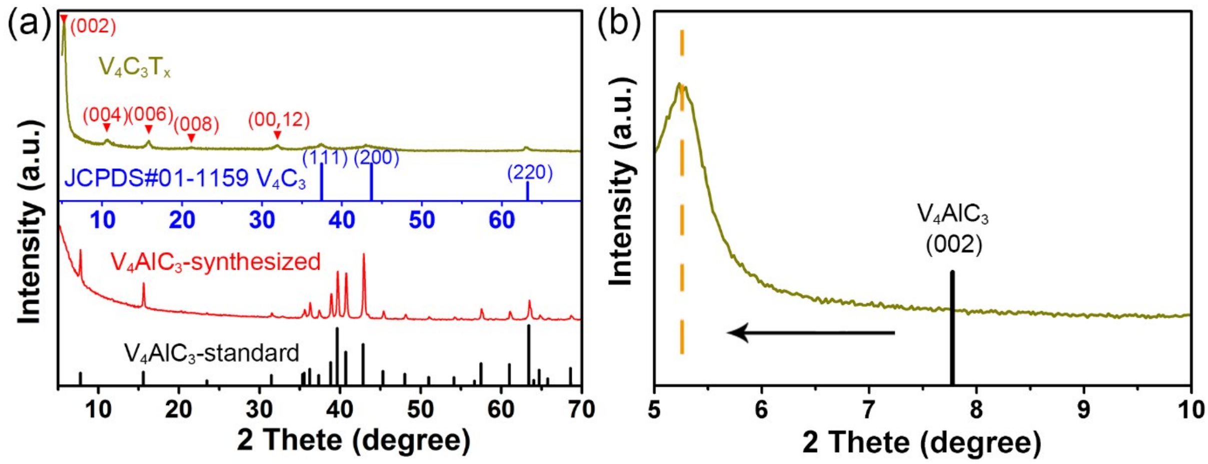

Figure S1. (a) XRD patterns of the synthesized V_4AlC_3 MAX and the exfoliated $V_4C_3T_x$ MXene. (b) The enlarge region shows the movement of (002) plane after exfoliation.

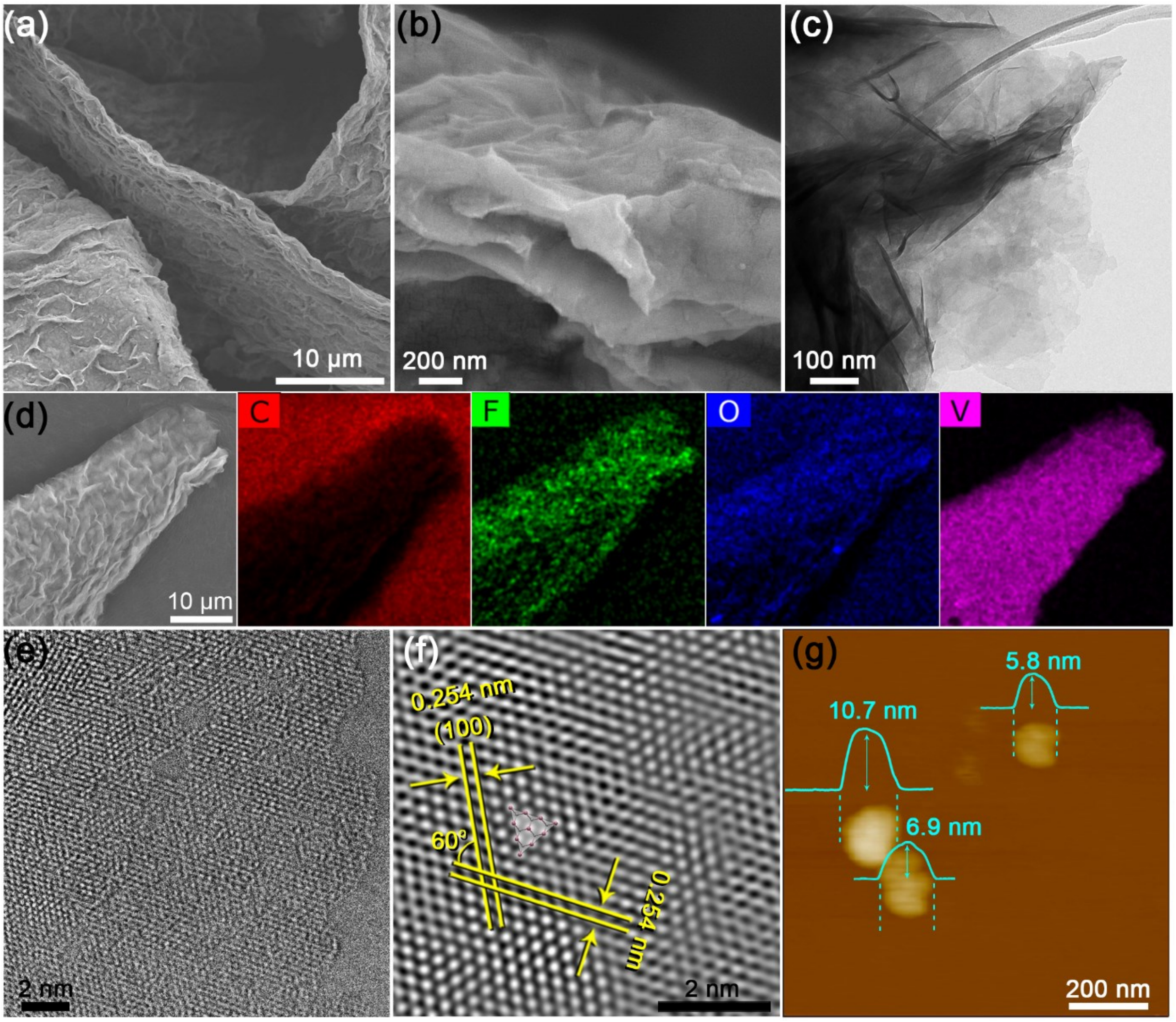

Figure S2. (a) Low-magnification and (b) high-magnification SEM image of the freeze dried $V_4C_3T_x$ MXene. (c) Low-magnification TEM images of an isolated freeze dried $V_4C_3T_x$ nanosheets. (d) The EDX elemental mapping of the freeze dried $V_4C_3T_x$ nanosheets. (e) HRTEM image and (f) the corresponding inverse FFT image of (e). (g) AFM images of the isolated $V_4C_3T_x$ nanosheets.

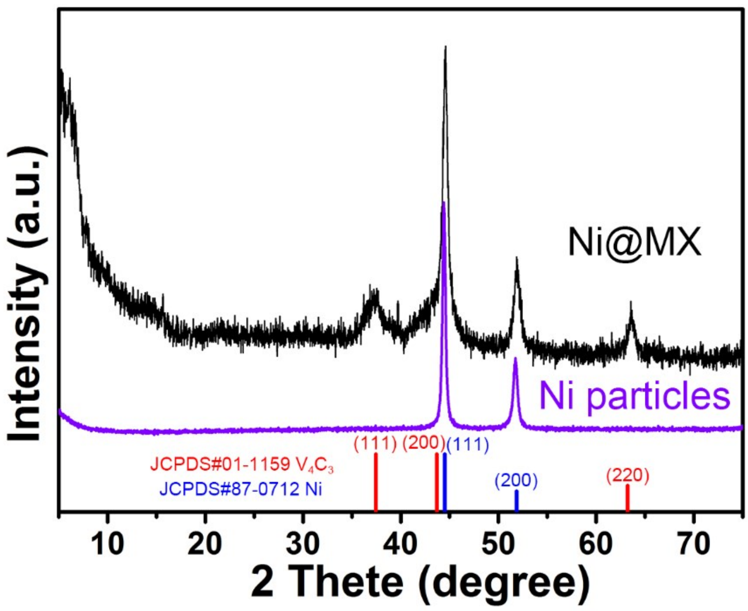

Figure S3. XRD patterns of the Ni@MX nanocomposite and the corresponding Ni particles prepared without MXene.

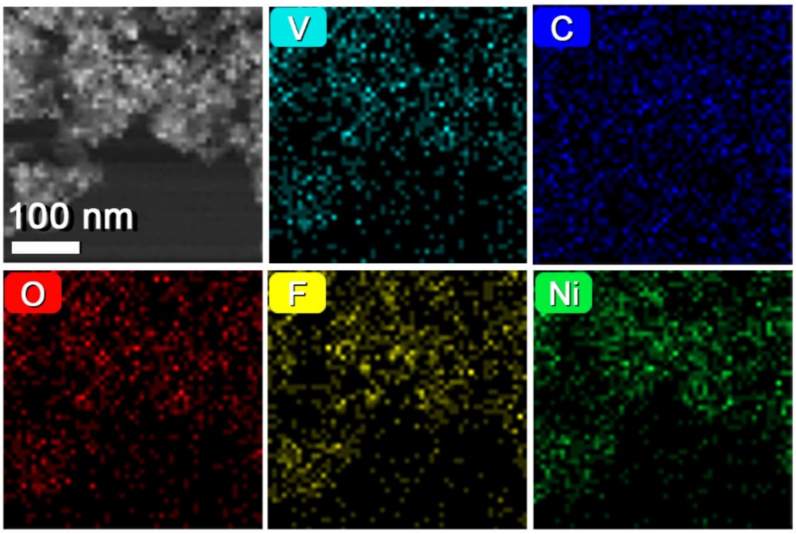

Figure S4. The EDX elemental mapping of Ni@MX nanocomposite.

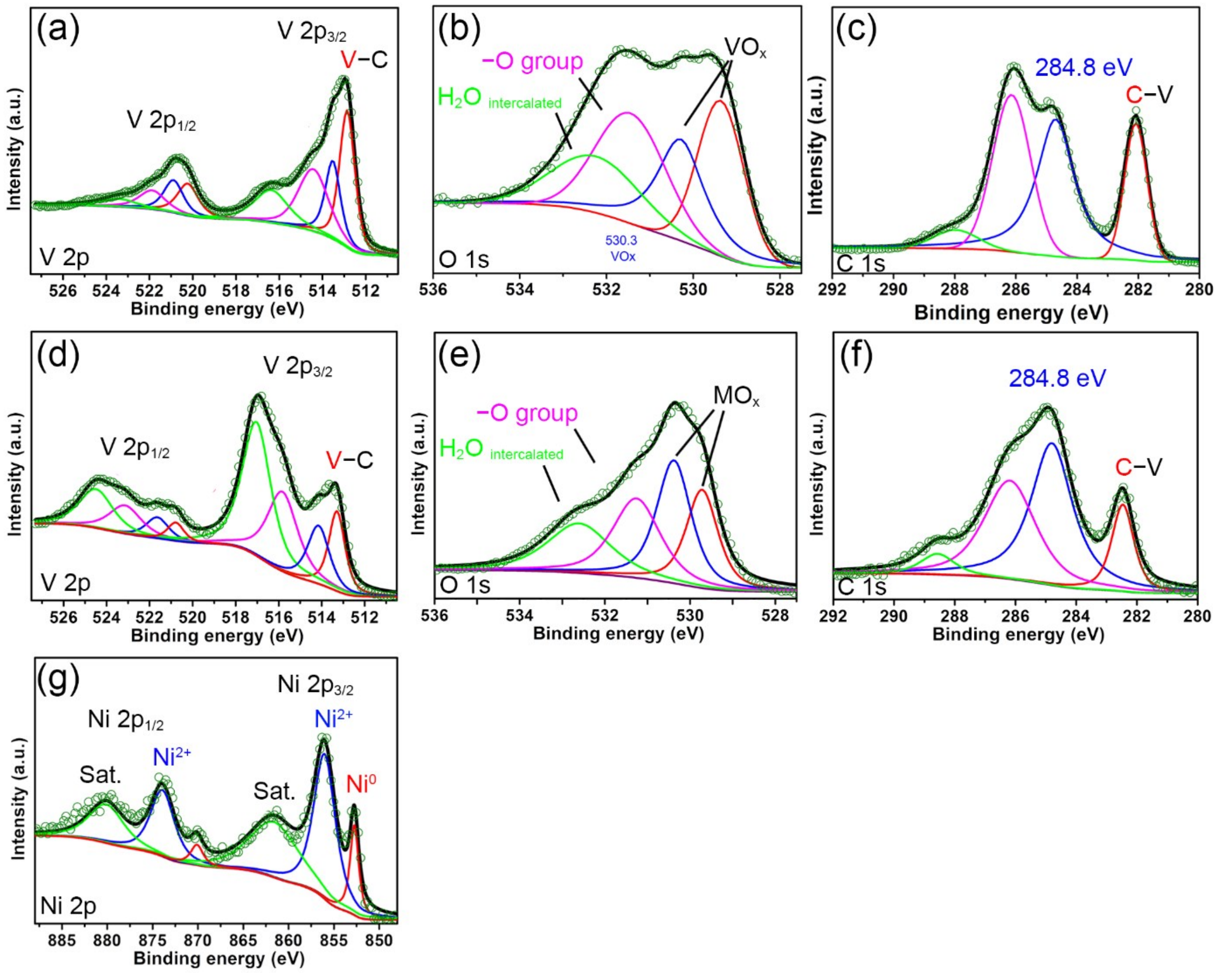

Figure S5. XPS spectra of the as-synthesized $V_4C_3T_x$ MXene and the Ni@MX nanocomposite: (a) V 2p, (b) O 1s and (c) C 1s spectra from $V_4C_3T_x$ MXene; (d) V 2p, (e) O 1s, (f) C 1s , and (g) Ni 2p from the Ni@MX nanocomposite.

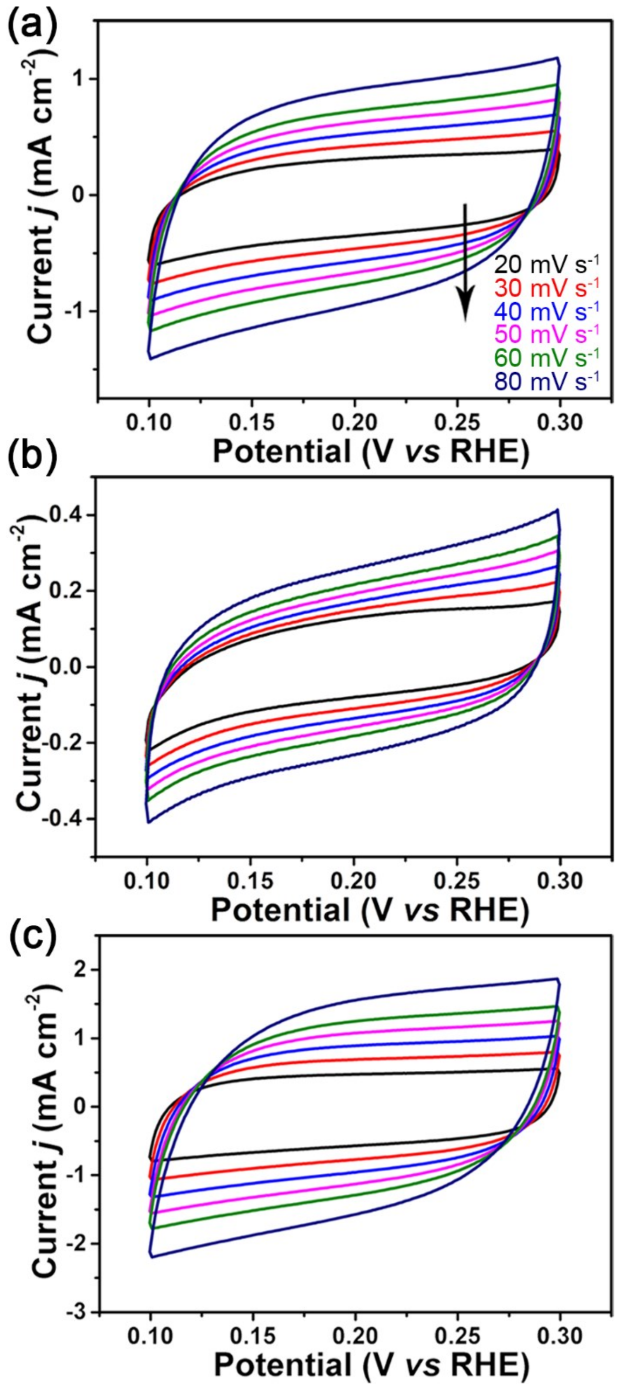

Figure S6. Cyclic voltammograms (CV) curves of (a) Ni@MX, (b) bare Ni particles, and (c) $V_4C_3T_x$ MXene, respectively. The CV curves are taken at various scan rates of 20, 30, 40, 50, 60 and 80 mV s^{-1} in 0.1 mol L^{-1} KOH solution.

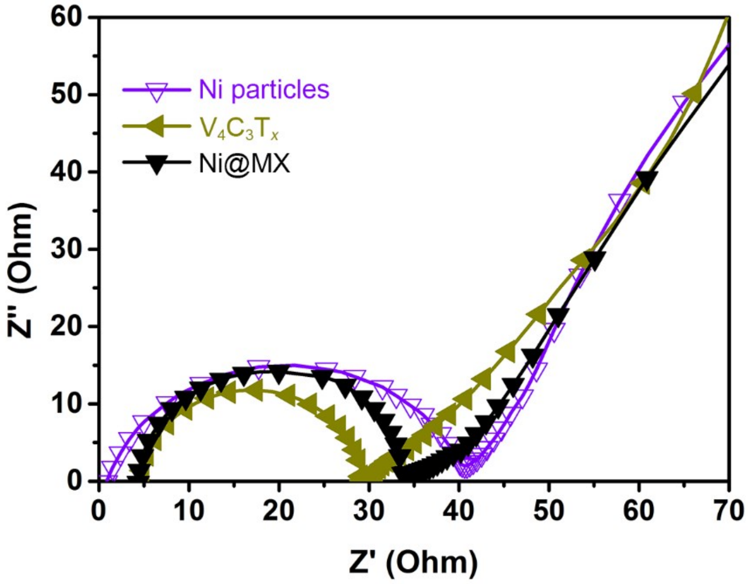

Figure S7. Fitted Nyquist plots of the electrodes modified by Ni@MX, Ni particles, and $V_4C_3T_x$ MXene measured at zero overpotential *vs*. RHE, respectively.

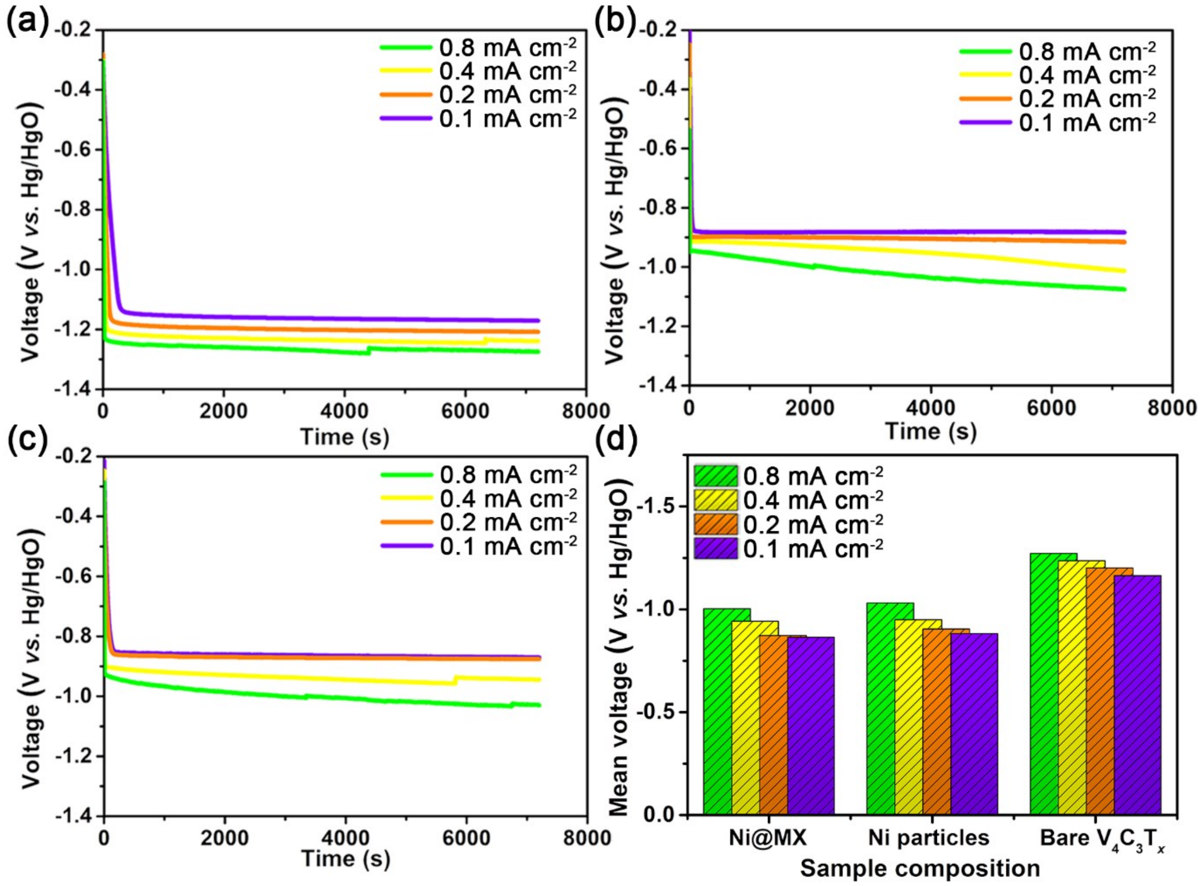

Figure S8. The chronopotentiometry curves of bare $V_4C_3T_x$ (a), Ni particles (b) and the Ni@MX nanocomposite (c) in N_2-saturated 0.1 mol L^{-1} KOH at different applied current density. (d) The mean voltages of the three samples.

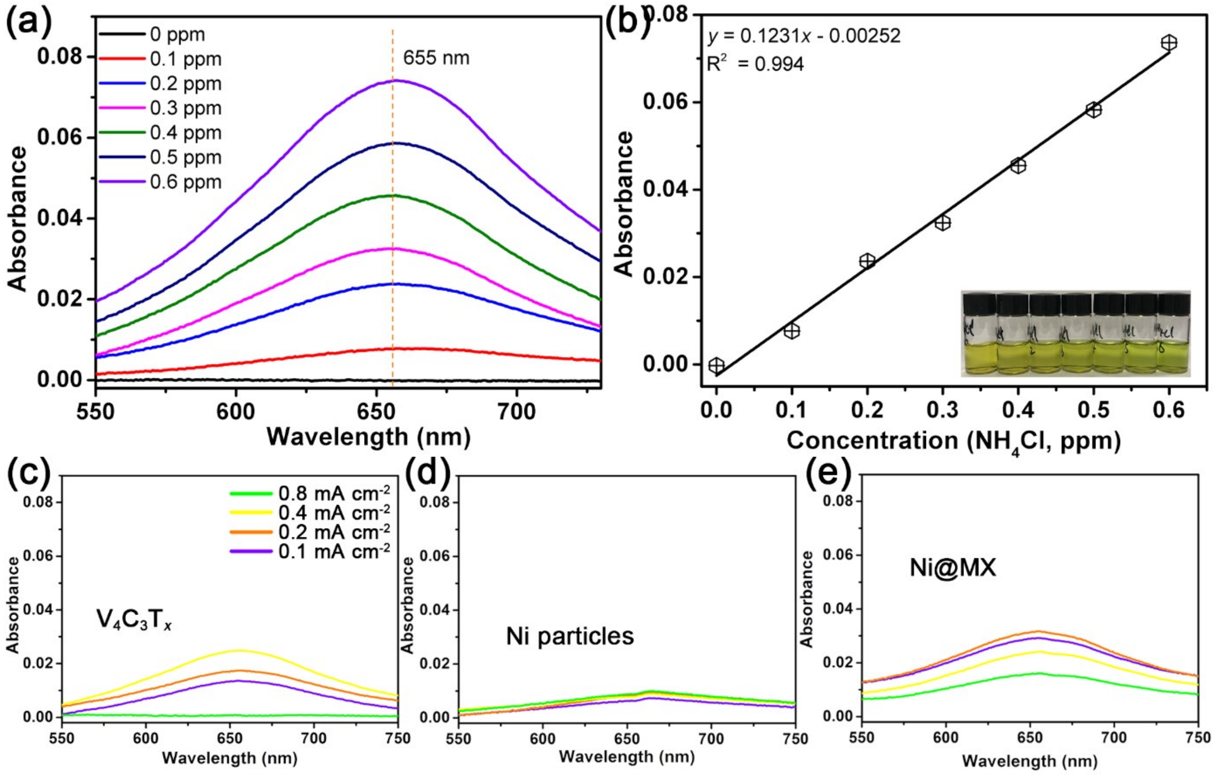

Figure S9. (a) UV/Vis absorption spectra of indophenol assays with NH_4^+ ions after incubated for 1 hours at room temperature. (b) Calibration curve used for calculation of NH_4Cl concentrations. (c-e) UV/Vis absorption spectra of indophenol assayed post-tested solution from bare $V_4C_3T_x$, Ni particles and the Ni@MX nanocomposite.

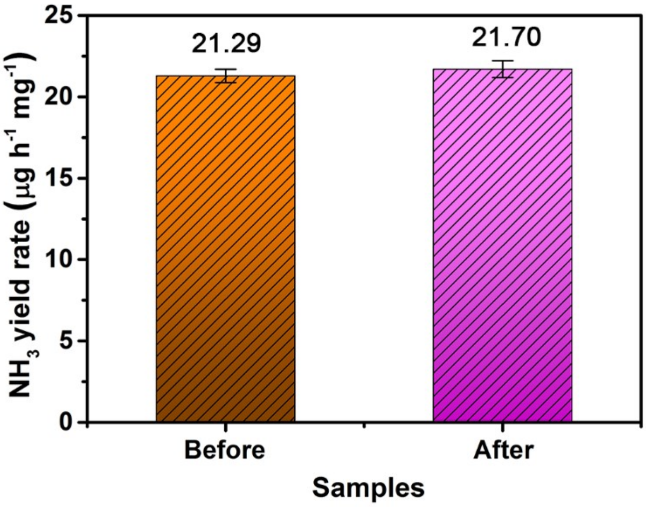

Figure S10. The normalized ammonia yield rate of the Ni@MX nanocomposite after 12 NRR cycles at 0.2 mA cm^{-2}.

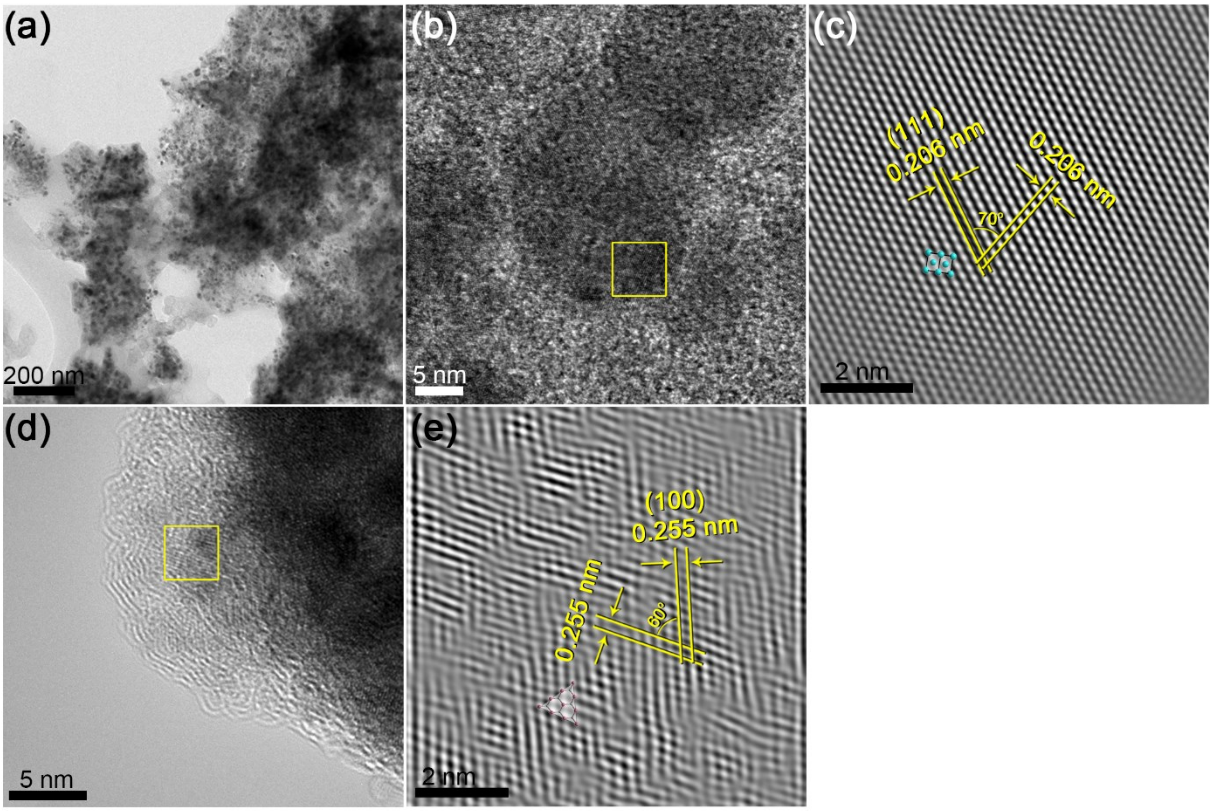

Figure S11. (a) TEM image of the Ni@MX nanocomposite after NRR process. (b) and (d) HRTEM images of the Ni nanoparticle and the $V_4C_3T_x$ MXene in the nanocomposite, respectively. (c) and (e) The i-FFT image of the selected area highlighted in (b) and (d), respectively.

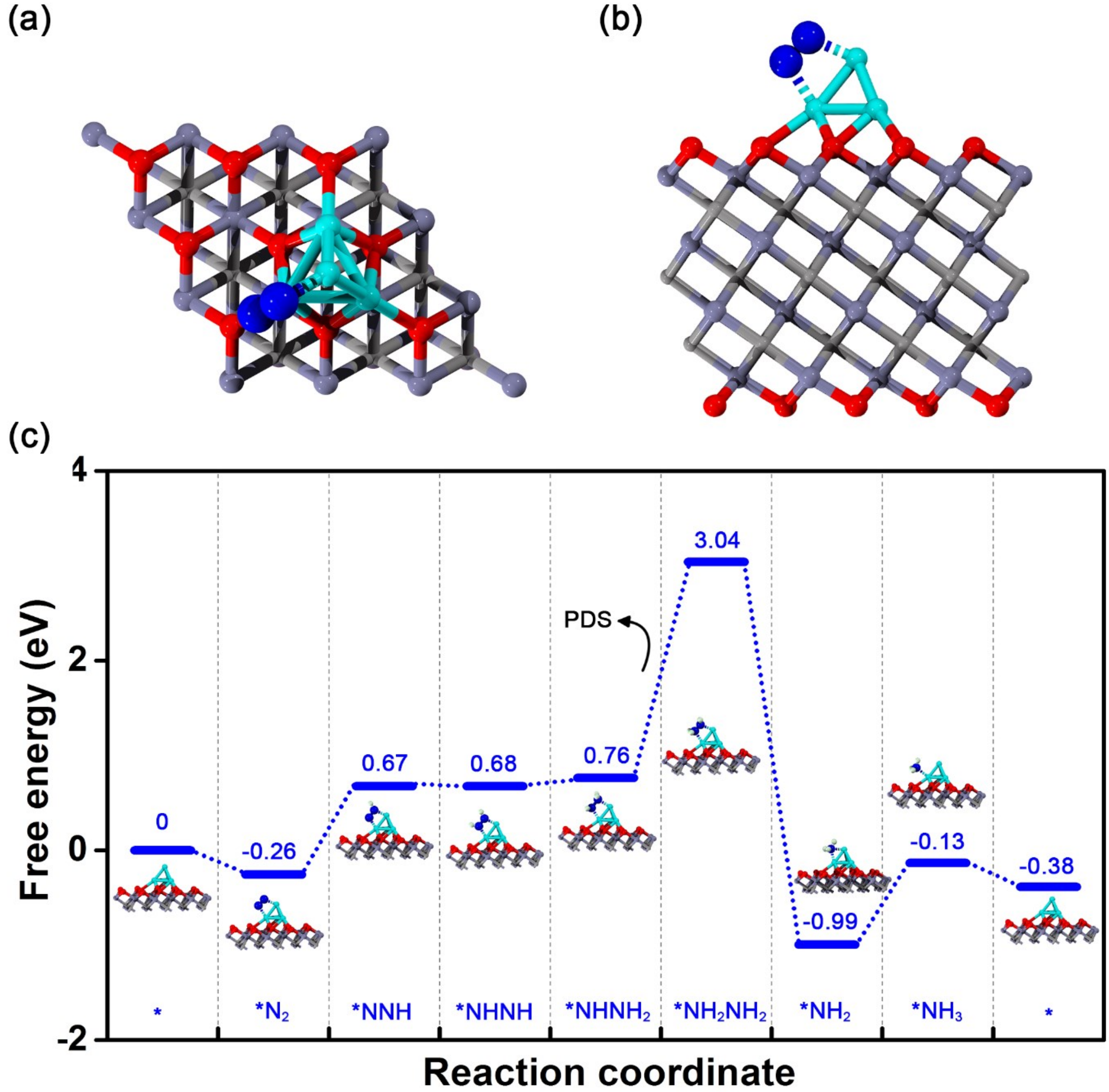

Figure S12. (a) Top and (b) side view of the atomistic configuration of Ni_4 nanocluster anchored on monolayer $V_4C_3O_2$ with enzymatically $*N_2$ adsorption on the Ni-Ni diatomic site. (c) Calculated free energy diagrams for NRR through the enzymatic mechanism on the Ni-Ni diatomic site of Ni_4 nanocluster.

Table S1. Comparison of NRR performances with reported electrocatalysts.

Catalyst	electrolyte	NH_3 Yield rate	NH_3 Faradic efficiency	Reference
$Ti_3C_2T_x$	0.5 mol L^{-1} Li_2SO_4	4.72 μg h^{-1} cm^{-2}	4.62%	[1]
$Ti_3C_2T_x$/FeOOH	0.5 mol L^{-1} Li_2SO_4	0.26 μg h^{-1} cm^{-2}	5.78%	
SA Ru-Mo_2CT_x	0.5 mol L^{-1} K_2SO_4	40.57 μg h^{-1} mg_{cat}^{-1}	25.77%	[2]
Mo_2CT_x	0.5 mol L^{-1} K_2SO_4	10.43 μg h^{-1} mg_{cat}^{-1}	7.73%	
Ru/C	0.5 mol L^{-1} K_2SO_4	19.56 μg h^{-1} mg_{cat}^{-1}	12.71%	
MoN NA/CC	0.1 mol L^{-1} HCl	18.42 μg h^{-1} cm^{-2}	1.15%	[3]
MnO_2–$Ti_3C_2T_x$	0.1 mol L^{-1} HCl	34.12 μg h^{-1} mg_{cat}^{-1}	11.39%	[4]
TiO_2/$Ti_3C_2T_x$	0.1 mol L^{-1} HCl	32.17 μg h^{-1} mg_{cat}^{-1}	~3%	[5]
Rh NCs/C	0.1 mol L^{-1} HCl	1.10 μg h^{-1} cm^{-2}	<1%	[6]
Rh/C	0.1 mol L^{-1} HCl	2.39 μg h^{-1} cm^{-2}	<1%	
Rh-Se NCs/C	0.1 mol L^{-1} HCl	17.75 μg h^{-1} cm^{-2}	13.3%	
Ru SAs/g-C_3N_4	0.5 mol L^{-1} NaOH	23.00 μg h^{-1} cm^{-2}	8.3%	[7]
Au NRs	0.1 mol L^{-1} KOH	1.65 μg h^{-1} cm^{-2}	~4%	[8]
W_2N_3	0.1 mol L^{-1} KOH	11.66 μg h^{-1} mg_{cat}^{-1}	11.67%	[9]
PdRu tripods	0.1 mol L^{-1} KOH	37.23 μg h^{-1} mg_{cat}^{-1}	1.85%	[10]
Ti_3C_2OH	0.1 mol L^{-1} KOH	1.71 μg h^{-1} cm^{-2}	7.01%	[11]
$V_4C_3T_x$	0.1 mol L^{-1} KOH	20.41 μg h^{-1} mg_{cat}^{-1} (3.26 μg h^{-1} cm^{-2})	3.80%	This work
Ni@MX	0.1 mol L^{-1} KOH	21.29 μg h^{-1} mg_{cat}^{-1} (3.41 μg h^{-1} cm^{-2})	8.04%	

References:

[1] Y. Luo, G.-F. Chen, L. Ding, X. Chen, L.-X. Ding, H. Wang, *Joule* **2019**, *3*, 279.
[2] W. Peng, M. Luo, X. Xu, K. Jiang, M. Peng, D. Chen, T.-S. Chan, Y. Tan, *Adv. Energy Mater.* **2020**, *10*, 2001364.
[3] L. Zhang, X. Ji, X. Ren, Y. Luo, X. Shi, A. M. Asiri, B. Zheng, X. Sun, *ACS Sustain. Chem. Eng.* **2018**, *6*, 9550.
[4] W. Kong, F. Gong, Q. Zhou, G. Yu, L. Ji, X. Sun, A. M. Asiri, T. Wang, Y. Luo, Y. Xu, *J. Mater. Chem. A* **2019**, *7*, 18823.
[5] Y. Fang, Z. Liu, J. Han, Z. Jin, Y. Han, F. Wang, Y. Niu, Y. Wu, Y. Xu, *Adv. Energy Mater.* **2019**, *9*, 1803406.
[6] C. Yang, B. Huang, S. Bai, Y. Feng, Q. Shao, X. Huang, *Adv. Mater.* **2020**, 2001267.
[7] B. Yu, H. Li, J. White, S. Donne, J. Yi, S. Xi, Y. Fu, G. Henkelman, H. Yu, Z. Chen, T. Ma, *Adv. Funct. Mater.* **2019**, *30*, 1905665.
[8] D. Bao, Q. Zhang, F.-L. Meng, H.-X. Zhong, M.-M. Shi, Y. Zhang, J.-M. Yan, Q. Jiang, X.-B. Zhang, *Adv. Mater.* **2017**, *29*, 1604799.
[9] H. Y. Jin, L. Q. Li, X. Liu, C. Tang, W. J. Xu, S. M. Chen, L. Song, Y. Zheng, S. Z. Qiao, *Adv. Mater.* **2019**, *31*, 8.
[10] H. Wang, Y. Li, C. Li, K. Deng, Z. Wang, Y. Xu, X. Li, H. Xue, L. Wang, *J. Mater. Chem. A* **2019**, *7*, 801.
[11] J. Xia, S.-Z. Yang, B. Wang, P. Wu, I. Popovs, H. Li, S. Irle, S. Dai, H. Zhu, *Nano Energy* **2020**, *72*, DOI: 10.1016/J.Nanoen.2020.104681.